Transport and Defect Mechanisms in Cuprous Delafossites. 2. $CuScO_2$ and $CuYO_2$

Brian J. Ingram, Bryan J. Harder, Nikolas W. Hrabe, and Thomas O. Mason*

Department of Materials Science and Engineering and Materials Research Center, Northwestern University, Evanston, Illinois 60208

Kenneth R. Poeppelmeier

Department of Chemistry and Materials Research Center, Northwestern University, Evanston, Illinois 60208

Received June 25, 2004. Revised Manuscript Received September 17, 2004

The delafossite structure (ABO_2) accommodates a wide range of transition and rare-earth cations on the B-site in combination with a short list of A-site cations. This paper reports the effects on defect chemistry and transport as a function of the B-site cation in copper-based delafossite materials, with $CuScO_2$ and $CuYO_2$ as examples. Large B-site cation delafossites exhibit small polaron conduction, a diffusion-limited conduction mechanism, with an activation energy approximately twice that of $CuAlO_2$ (0.22 eV vs 0.14 eV, respectively). The mobility for these materials is found to be <1 cm^2 V^{-1} s^{-1}, further evidence of small polaron conduction. The majority defect species is highly dependent on the B-site cation, such that $CuScO_2$ and $CuYO_2$ are dominated by extrinsic defects (acceptor doping) and free oxygen interstitials, whereas off-stoichiometry dominates $CuAlO_2$. Dopant solubility is shown to be 1% for bulk $CuScO_2$ samples and lower in $CuYO_2$.

Introduction

As discussed in Part 1 of this series,[1] the delafossite structure, with the general formula $A^{1+}B^{3+}O_2$, has been suggested as a candidate for p-type transparent conducting oxide (TCO) materials (i.e., $CuAlO_2$[2]). TCOs are utilized as transparent electrodes in a wide range of applications such as flat panel displays, electrochromic mirrors and windows, and photovoltaic devices. Currently all commercially available TCOs are n-type, in which electrons are the dominant charge carrier. The development of a high figure-of-merit p-type TCO, in combination with their n-type counterparts, would advance innovative devices such as improved flat-panel displays, ultra-violet emitting diodes, and heterojunctions for solar cells, as well as all-oxide (transparent) semiconductor devices such as diodes and transistors.

The transport and defect mechanisms in $CuAlO_2$ were considered in Part 1.[1] The influence of the B-cation size (B = Sc, Y) on defects and transport in delafossites is reported in the current paper. It should be noted that the c-lattice parameter of $A^{1+}B^{3+}O_2$ delafossites is highly dependent on the A-site cation radius (i.e., Cu^{1+} or Ag^{1+}), which affects the A−O distance. This variable, however, has little effect on the a-lattice parameter (equivalent to the A−A distance), which to a large degree is only dependent on the B-site cation (especially in $CuBO_2$).

Despite the favorable structural properties, experimental and theoretical investigations have reported low mobility and hole contents for $CuAlO_2$,[2−9] and small polaron conduction (a diffusion-limited transport mechanism) has been established, suggesting a room-temperature mobility less than 1 cm^2 V^{-1} s^{-1}.[10] Extrinsic acceptor-doping has proven difficult in $CuAlO_2$ and oxidation anneals have been shown to have little effect on the hole concentration.[1]

Cu-based delafossite materials possessing larger B-site cations have two advantages over $CuAlO_2$, leading to higher hole concentrations: increased capacity for extrinsic doping on the B-site and the possibility of oxygen interstitials in the Cu-plane. It has been previously shown that $CuY_{1-x}Ca_xO_{2+\delta}$ and $CuSc_{1-x}Mg_xO_{2+\delta}$ can exhibit oxygen contents well in excess of $\delta = 0.5$,[11−14] supported by theoretical calculations of the

* To whom correspondence should be addressed. E-mail: t-mason@northwestern.edu.

(1) Ingram, B. J.; Gonzalez, G. B.; Mason, T. O.; Shahriari, D. Y.; Barnabe, A.; Ko, D.; Poeppelmeier, K. R. Transport and defect mechanisms in cuprous delafossites. Part 1: A comparison of hydrothermal and standard solid-state synthesis in $CuAlO_2$. *Chem. Mater.* **2004**, *16*, 5616−5622.

(2) Kawazoe, H.; Yasukawa, M.; Hyodo, H.; Kurita, M.; Yanagi, H.; Hosono, H. *Nature* **1997**, *389*, 939−942.

(3) Benko, F. A.; Koffyberg, F. P. *J. Phys. Chem. Solids* **1984**, *45* (1), 57−59.

(4) Stauber, R. E.; Perkins, J. D.; Parilla, P. A.; Ginley, D. S. *Electrochem. Solid State Lett.* **1999**, *2* (12), 654−656.

(5) Gong, H.; Wang, Y.; Luo, Y. *Appl. Phys. Lett.* **2000**, *76* (26), 3959−3961.

(6) Gao, S.; Zhao, Y.; Gou, P.; Chen, N.; Xie, Y. *Nanotechnology* **2003**, *14*, 538−541.

(7) Ohashi, M.; Iida, Y.; Morikawa, H. *J. Am. Ceram. Soc.* **2002**, *85* (1), 270−272.

(8) Wang, Y.; Gong, H. *Chem. Vap. Deposition* **2000**, *6* (6), 285−288.

(9) Lee, M. S.; Kim, T. Y.; Kim, D. *Appl. Phys. Lett.* **2001**, *79* (13), 2028−2030.

(10) Ingram, B. J.; Mason, T. O.; Asahi, R.; Park, K. T.; Freeman A. J. *Phys. Rev. B* **2001**, *64* (15), 155114−1, 15114−7.

10.1021/cm048982k CCC: $27.50
Published on Web 12/02/2004

electronic structure of $CuYO_{2+\delta}$;[15] however, structural studies indicate a rhombohedral structure different from 3R delafossite becomes stable beyond $\delta = 0.5$.[16] At the time of this paper the highest reported conductivity value for the delafossite materials is ~40 S/cm for Mg-doped $CuScO_2$ following an oxygen anneal.[17] The current research has focused on the transport mechanism and defect structures of the delafossite structure as the size of the B-site cation is increased from $Al^{(IV)}$ to $Sc^{(IV)}$ and $Y^{(IV)}$ ($r = 0.675$, 0.870, and 1.032 Å, respectively.[18]).

Experimental Procedures

Solid bulk samples were produced by conventional high-temperature solid-state reaction. Component oxides (Adrich Chemical Co., Milwaukee, WI; 99.99−99.9999%) were combined in stoichiometric ratio and mixed in an agate mortar and pestle under acetone until a homogeneous mixture was obtained. Doping of the delafossite phase was assumed to take place on the B-site, and therefore a proper amount of B_2O_3 was replaced with B′O or B′CO_3 (in which B′ = Mg or Ca, respectively) satisfying the formula $CuB_{1-x}B'_xO_2$. To ensure accurate molar proportion of cationic species, the component oxides were dried in a furnace at 400 °C for 12 h and stored in a desiccator. In the case of $CuScO_2$, copper (I) oxide was found to be a suitable source of copper; however, in the case of $CuYO_2$, copper (II) oxide provided better results.

Once a homogeneous mixture was obtained, pellets were uniaxially pressed at ~175−400 MPa and surrounded by a small amount of sacrificial powder of the same nominal composition to prevent reaction between the pellet and the crucible. For $CuScO_2$ the pellets were then heated in air to 1100 °C for 24 to 36 h in high-purity Al_2O_3 crucibles, and subsequently quench-cooled in air. The pellets were weighed before and after firing to estimate weight loss, and analyzed by X-ray diffraction to verify phase purity. This process of firing and phase analysis was repeated until an X-ray phase-pure sample of $CuBO_2$ was achieved, which typically took two firing cycles. The software package FullProf 2000[19] was used for lattice parameter determinations.

For synthesis of $CuYO_2$, the pressed homogenized mixture was fired at 1000 °C in air for 24 h to form the thermodynamically stable Cu^{2+} phase (orthorhombic $Cu_2Y_2O_5$). This step appeared to be necessary due to the sluggish rate of formation of the delafossite phase in this system.[20] The $Cu_2Y_2O_5$ phase was subsequently reduced at 1000 °C under flowing Ar. Isolation of single-phase polytypes (2H or 3R) was difficult; consequently, the undoped Y- and Sc-based samples consisted of 3R and 2H polytypes (approximately 70% and 30%, respectively), most likely corresponding to stacking faults. Acceptor-doping tended to stabilize the 2H polytype relative to the 3R.

Room- and high-temperature conductivity and thermopower measurements were collected to analyze the defect and transport properties of the delafossite compounds. The method described by Hong et al.[21] was employed in which the natural thermal gradient of the furnace was exploited for thermopower determination. The conductivity was measured by averaging forward and reverse biased current results to remove thermal emf contributions. It was found that electrical contacts were improved by sputtering 10−20 nm of gold onto the surface of the ceramic bar at the point of electrical contact, ensuring quality contact between gold wire electrodes and the sample at high temperatures. At high temperature, thermal equilibrium was established by monitoring the time-dependence of in situ electrical properties.

Samples were typically between 60 and 70% dense; therefore the conductivity was corrected for porosity by using the Brueggeman symmetric medium equation (3:3 connectivity of both solid phase and residual porosity) as described by McLachlan et al.[22]

$$\sigma_{\text{measured}} = \sigma_{\text{actual}}[1 - {}^3/_2 f] \quad (1)$$

where f is the volume fraction of porosity ($0 \le f \le 0.4$). Density corrections were found to increase the measured conductivity by a factor of 1.8 to 2.5. In addition, the anisotropic nature of the delafossite structure was taken into consideration, in which current travels predominantly in the basal-plane (A-cation planes).[9] It is believed that the existence of two polytypes (3R and 2H), which alters the stacking along the c-axis, has little effect on the measured polycrystalline conductivity values, which is ~$^2/_3$ σ_{ab}, where σ_{ab} is the conductivity along the basal-plane.[23]

The geometry of the setup was expected to be the primary source of error for conductivity measurements; therefore, the systematic error on each conductivity measurement was approximated by the following:

$$\%\ \text{error} \approx 2d/a \quad (2)$$

where d was the diameter of the wire contacts and a was the inter-electrode spacing between the contacts.[21] This provides the systematic error (specimen-to-specimen). Once electroded, however, a given sample will have a much smaller random error (datum-to-datum) arising from instrumental uncertainties.

Results

Transport Mechanism. The temperature dependence of the electrical properties of undoped $CuScO_2$ and $CuYO_2$ is shown in Figures 1 and 2, respectively, collected at $\log(pO_2) \approx -3.9$. The systematic error, as described by eq 2, representing uncertainty in the location of the entire data set, is illustrated by an error bar to the right of the data, whereas random error, contributing to scatter around the least-squares linear fit, is on the order of the symbol size or smaller. The relatively narrow temperature ranges (in Figures 1−4) and oxygen partial pressure ranges (in Figures 5 and 6) are due to the limited stability ranges of the compounds and/or reaction with the Au electrodes above 850−900 °C. For example, $CuYO_2$ oxidizes to orthorhombic $Cu_2Y_2O_5$ below 670−800° C, depending upon the pO_2 imposed.

(11) Cava, R. J.; Zandbergen, H. W.; Ramirez, A. P.; Takagi, H.; Chen, C. T.; Krajewski, J. J.; Peck Jr, W. F.; Waszczak, J. V.; Meigs, G.; Roth, R. S.; Schneemeyer, L. F. *J. Solid State Chem.* **1993**, *104*, 437−452.
(12) Duan, N.; Sleight, A. W.; Jayaraj, M. K.; Tate, J. *Appl. Phys. Lett.* **2000**, *77* (9), 1−2.
(13) Trari, M.; Töpfer, J.; Doumcerc, J. P.; Rouchard, M.; Ammar, A.; Hagenmuller, P. *J. Solid State Chem.* **1994**, *111*, 104−110.
(14) Van Tendeloo, G.; Garlea, O.; Darie, C.; Bougerol-Chaillout, C.; Bordet, P. *J. Solid State Chem.* **2001**, *156*, 428−436.
(15) Mattheiss, L. F. *Phys. Rev. B.* **1993**, *48* (24), 18300−18303.
(16) Garlea, O.; Darie, C.; Bougerol, C.; Isnard, O.; Bordet, P. *Solid State Sci.* **2003**, *5*, 1095−1104.
(17) Nagarajan, R.; Duan, N.; Jayaraj, M. K.; Li, J.; Vanaja, K. A.; Yokochi, A.; Draeseke, A.; Tate, J.; Sleight, A. W. *Int. J. Inorg. Mater.* **2001**, *3*, 265−270.
(18) Shannon, R. D.; Prewitt, C. T. *Acta Crystallogr.* **1969**, *B25*, 925−946.
(19) Rodríguez-Carvajal, J. *FullProf 2000*; Laboratoire Léon Brillouin, Saclay, France, 2001 (http://www-llb.cea.fr/fullweb/winplotr/winplotr.htm).
(20) Ishiguro, T.; Ishizawa, N.; Mizutani, N.; Kato, M. *J. Solid State Chem.* **1983**, *49*, 232−236.
(21) Hong, B.-S.; Ford, S. J.; Mason, T. O. *Key Eng. Mater.* **1997**, *125−126*, 163−186.
(22) McLachlan, D. S.; Blaszkiewicz, M.; Newnham, R. E. *J. Am. Ceram. Soc.* **1990**, *73* (8), 2187−2202.
(23) Routbort, J. L.; Rothman, S. J. *J. Appl. Phys.* **1994**, *76* (10), 5615−5628.

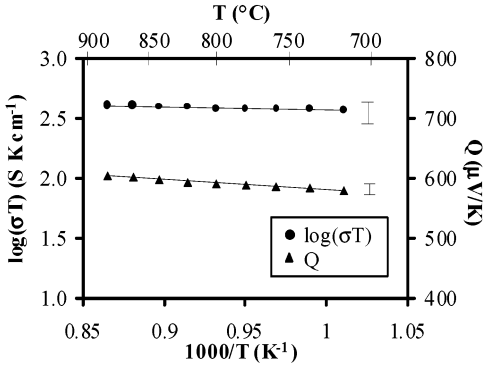

Figure 1. Temperature dependence of the electrical properties of $CuScO_2$. The systematic error is represented by the error bar to the right of the data, whereas the random error is on the order of symbol size.

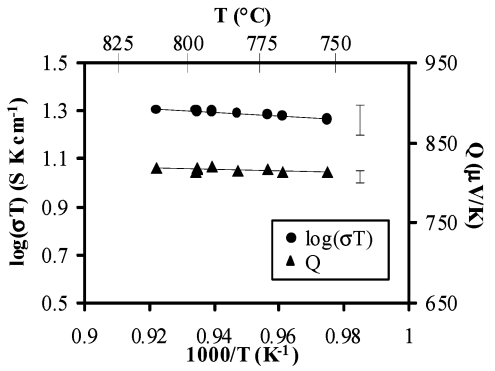

Figure 2. Temperature dependence of the electrical properties of $CuYO_2$. The systematic error is represented by the error bar to the right of the data, whereas the random error is on the order of symbol size.

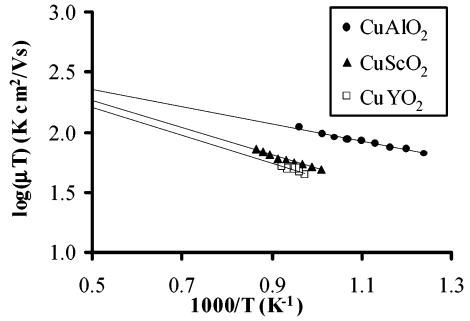

Figure 3. Mobility−temperature product as a function of temperature is shown to compare small polaron behavior among $CuAlO_2$, $CuScO_2$, and $CuYO_2$. The hopping energy is given by the slope, and the preexponential constant, μ_o, (see eq 3) is given by the intercept.

As can be seen in Figures 1 and 2, the thermopower values are positive, verifying p-type conduction, and are slightly temperature dependent, suggesting decreasing hole concentrations with increasing temperature. Despite the trend in hole concentration, the conductivity exhibits the opposite trend, indicating an activated mobility, as in $CuAlO_2$,[10] where the mobility may be written as

$$\mu = \frac{\mu_o}{T}\exp\left(\frac{-E_h}{k_B T}\right) = \frac{g(1-c)ea^2\nu}{k_B T}\exp\left(\frac{-E_h}{k_B T}\right) \quad (3)$$

where μ_o is the preexponential factor, E_h is the hopping energy, g is a geometric factor; $(1 - c)$ is the fraction of unoccupied states; e is the unit of electron charge; a is jump distance; ν is the optical phonon frequency responsible for hopping; and k_B is Boltzmann's constant.

Assuming a nondegenerate semiconductor for which Boltzmann statistics are applicable, the thermoelectric coefficient can be directly related to the hole concentration by the following equation:[24]

$$Q = \pm\frac{k_B}{e}\left(\ln\left(\frac{N(\epsilon)}{p}\right) + A\right) \quad (4)$$

where $N(\epsilon)$ is the effective density of states (DOS) at

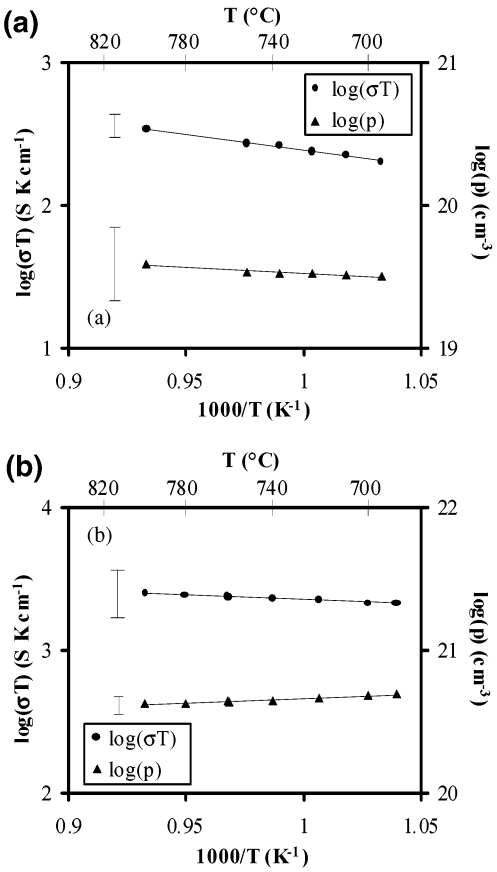

Figure 4. Temperature dependence of the electrical properties of 5% (a) Mg-doped $CuScO_2$ and (b) Ca-doped $CuYO_2$. The systematic error is represented by the error bar to the right of the data, whereas the random error is on the order of symbol size.

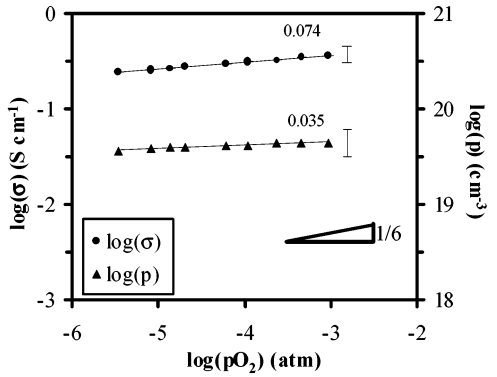

Figure 5. pO_2-Dependence of the electrical properties of $CuScO_2$. The systematic error is represented by the error bar to the right of the data, whereas the random error is on the order of symbol size. The slopes are given by the numerical values and a $^1/_6$ slope is displayed for comparison.

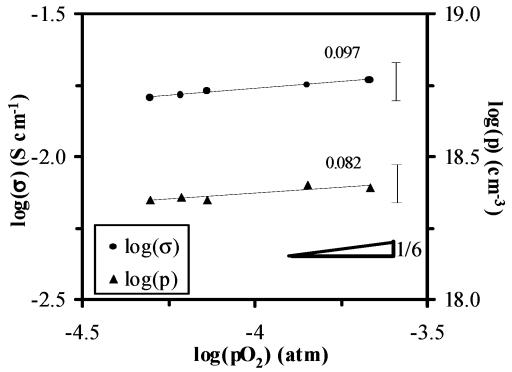

Figure 6. pO_2-Dependence of the electrical properties of $CuYO_2$. The systematic error is represented by the error bar to the right of the data, whereas the random error is on the order of symbol size. The slopes are given by the numerical values and a $^1/_6$ slope is displayed for comparison.

the transport level and p is the charge carrier concentration. For small polarons $A \approx 0$ and the DOS can be taken as the total atomic Cu-sites available ($N \approx 10^{22}$ cm^{-3}). Equation 4 can therefore be rewritten as a function of the ratio of available sites, $(1 - c)N$, to filled sites, cN, in the following form:

$$Q = + \frac{k_B}{e} \ln\left(\frac{\beta(1-c)}{c}\right) \tag{5}$$

where β, the spin degeneracy factor, is typically 2, and c is the fraction of sites occupied by holes. The positive sign in eq 5 is determined by the charge carrier (i.e., Cu^{2+}) and all values listed in this study are based on this model; however, it should be noted that a similar case can be derived in which the polaron forms around a trapped electron (i.e., Cu^{1+} polarons on Cu^{2+} sites) by changing the sign of eq 5 and redefining the ratio of available to filled sites as $c/(1 - c)$. Positive and negative Seebeck coefficients (p-type and n-type conduction, respectively) are possible for each model depending on the ratio of available to filled states, with an approximate 25% difference in calculated hole concentration.

Careful consideration was taken to establish the relative contributions of carrier content and mobility to the conductivity since the carrier concentration can exhibit a slight temperature dependence as seen in Figures 1 and 2. The hopping energy is therefore calculated from

$$k_B\left[\left(\frac{\partial \ln \sigma T}{\partial(1/T)}\right) - \left(\frac{\partial \ln cN}{\partial(1/T)}\right)\right] = - E_h \tag{6}$$

The small polaron hopping energies for $CuScO_2$ and $CuYO_2$ have been determined from eq 6 as 0.22 ± 0.04 and 0.23 ± 0.05 eV, respectively. The mobilities at 740 °C are consistent with the small polaron model (0.05 $cm^2\ V^{-1}\ s^{-1}$ for $CuScO_2$ and 0.04 $cm^2\ V^{-1}\ s^{-1}$ for $CuYO_2$), and are about half the value of $CuAlO_2$. Based upon eq 3 additional terms can be evaluated, i.e., the preexponential constants, μ_o, calculated from the data in Figures 1 and 2 are 660 and 610 K $cm^2\ V^{-1}\ s^{-1}$ for $CuScO_2$ and $CuYO_2$, respectively, comparing favorably with the value for $CuAlO_2$ of 500 K $cm^2\ V^{-1}\ s^{-1}$.[10] Based on these values, the optical phonon frequency for both $CuScO_2$ and $CuYO_2$ is approximately 2.7×10^{13} s^{-1}, which is a reasonable value.

Table 1. Summary of the Electrical Properties of $CuBO_2$ at 740 °C and $\log(pO_2) \approx -3.9$

B =	Sc	$Sc_{0.95}Mg_{0.05}$	Y	$Y_{0.95}Ca_{0.05}$
σ (S/cm)	0.37	2.28	0.018	0.26
μ ($cm^2V^{-1}s^{-1}$)	0.05	0.03	0.04	0.05
$p \times 10^{20}$ (cm^{-3})	0.45	4.48	0.026	0.33
E_h (eV)	0.22	0.25	0.23	0.28
μ_o ($Kcm^2V^{-1}s^{-1}$)	660	570	610	1130

The mobility−temperature product vs reciprocal temperature for $CuBO_2$ (B = Al,[10] Sc, and Y) is reviewed in Figure 3, in which the values are established by small polaron analysis. It can be seen that the delafossite materials under investigation share the same transport mechanism, with similar values of μ_o (500−660 K cm^2 V^{-1} s^{-1}) and an increasing E_h with B-site cation radius. Furthermore, low-temperature studies have shown variable range hopping characteristics ($\log(p) \approx T^{-1/4}$) in both $CuScO_2$[12] and $CuYO_2$,[11] further supporting the polaron character of these materials.

Additionally, the effects of doping on the transport mechanism in delafossite materials were considered. The temperature-dependences of Mg-doped $CuScO_2$ and Ca-doped $CuYO_2$ are shown in Figure 4a and b, respectively, verifying small polaron conduction as described in the undoped materials. Activation energies are comparable to undoped specimens. Table 1 summarizes the transport properties of doped and undoped $CuScO_2$ and $CuYO_2$ specimens at ~740 °C and $\log(pO_2) \approx -3.9$.

Defect Structure. The defect chemistry of cuprous-delafossites with larger B-site cations (i.e., $CuScO_2$ and $CuYO_2$) was also investigated. Small pO_2 excursions were made at constant temperature (800 °C) with the results shown in Figures 5 and 6 for $CuScO_2$ and $CuYO_2$, respectively. The thermopower values were converted to hole concentration as per eq 5. A $^1/_6$ slope, in accordance with the following equations

$$^1/_2\ O_{2(g)} \rightarrow O_i'' + 2h^\bullet \tag{7a}$$

$$\log(p) = constant + {}^1/_6 \log(pO_2) \tag{7b}$$

has been indicated for comparison to the experimentally determined slopes. Additionally, the numerical values of the fitted slopes are labeled. The p-type character of the system is confirmed through a positive Seebeck coefficient as well as a slight increase in conductivity and hole concentrations with oxygen partial pressure. In Part 1, $CuAlO_2$ was shown to exhibit negligible pO_2-dependence of conductivity and hole concentration;[1] likewise, the electrical properties for both $CuScO_2$ and $CuYO_2$ exhibit distinct slopes less than $^1/_6$. The inclusion of oxygen interstitials in both the Sc- and Y-compounds is well-known;[11,12] therefore, a more prominent pO_2-dependence on the electrical properties is expected under more oxidizing conditions. Under the experimental conditions the Sc- and Y-systems may exist between two Brouwer regimes: an intrinsic pO_2-dependent regime (e.g., $2[O_i''] = p$) and a regime in which the hole concentration is fixed (e.g., $[A_Y']$ or $[V_{Cu}'] = p$). Based on Figures 5 and 6, oxygen interstitials are not the

(24) Ioffe, A. F. *Physics of Semiconductors;* Infosearch: London, 1960.

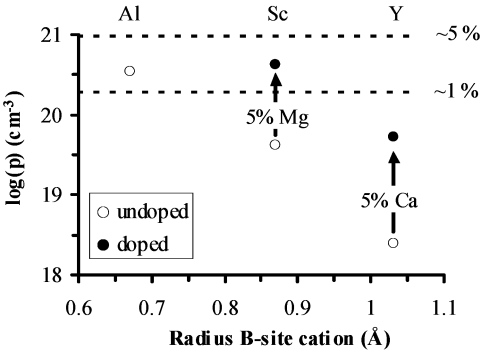

Figure 7. Review of the hole concentrations at $\log(pO_2) = -4$ and 800 °C for doped and undoped samples. Estimated hole concentrations for 1 and 5% doping are designated with dashed lines.

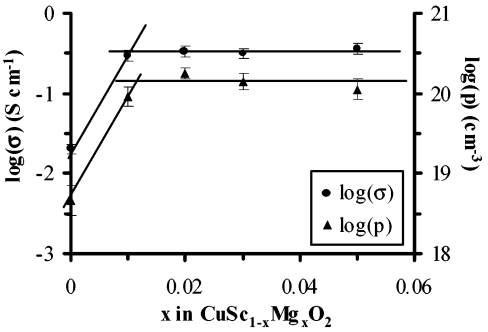

Figure 8. Room-temperature electrical properties of $CuSc_{1-x}Mg_xO_2$ as a function of x. Saturation of the electrical properties is attained between $x = 0.1$ and 0.2. The hole concentration is determined by eq 5 from thermopower measurements and saturates at ~1% doping level. The estimated error in x is found to be on the order of symbol size.

dominant defect in $CuScO_2$ or $CuYO_2$ under the experimental conditions.

The hole concentration vs B-site radius in the undoped delafossites under similar conditions (~800 °C, $\log(pO_2) \approx -4$) is summarized in Figure 7 as open circles, which further suggests that oxygen interstitials do not dominate as the B-site radius increases. While undoubtedly present in $CuScO_2$ and $CuYO_2$ at low temperatures and high oxygen pressures, free oxygen interstitials (O_i'') must not be present in significant quantities at elevated temperatures under the pO_2 values employed in the present study.

The contribution of unintentional impurity dopants to the hole concentration was also considered. Tramp impurity surveys (Chicago Spectro Services Laboratory, Inc.) were performed on $CuScO_2$ and $CuYO_2$ (CSSL 10.4.5, ASTM E1085). Effective doping levels were determined by summing the contributions of each impurity species, assuming fully ionized impurity substitution on the B^{3+}-site. Tramp impurity levels in $CuScO_2$ contribute $<2.0 \times 10^{18}$ holes cm^{-3} compared to the hole concentration in Figure 7 ($\sim 4.0 \times 10^{19}$ cm^{-3}) and, therefore, do not significantly affect the subsequent electrical properties. On the other hand, the impurity level in $CuYO_2$ corresponds to $<1.0 \times 10^{19}$ cm^{-3}, compared to the hole concentration shown in Figure 7 for undoped $CuYO_2$ ($\sim 2.5 \times 10^{18}$ cm^{-3}), suggesting that tramp impurities may have played a role in determining the hole concentration of undoped $CuYO_2$.

To further appreciate the trend seen for the undoped samples in Figure 7, cation off-stoichiometry was considered. As discussed in Part 1,[1] Al^{3+} substitutes on the linearly coordinated Cu-sites of $CuAlO_2$ and is stabilized by the formation of a pseudo-tetrahedral site with the addition of two tightly bound oxygen interstitials. This defect complex serves as an acceptor, as seen below for a general case:

$$2[(B_{Cu}^{\bullet\bullet}2O_i'')''] = p \qquad (8)$$

Neutron and X-ray refinements[1] provide convincing evidence of this complex in $CuAlO_2$; however, based on the decreased carrier concentrations seen in Figure 7, the complex appears less prevalent in $CuScO_2$ and $CuYO_2$. Despite the openness of the structure within the Cu-plane in large B-site cation systems, two factors contribute to the apparent reduction in the stability of the complex relative to $CuAlO_2$. The Cu−O distance (related to the c-lattice parameter) is fixed by the A-cation size and will not accommodate larger B-cations. More significantly, Sc and Y tend to be unstable in low coordination sites[25] such as required by the $(B_{Cu}^{\bullet\bullet}2O_i'')''$ species.

Although undoped $CuScO_2$ and $CuYO_2$ possess high-temperature electrical properties inferior to those of their $CuAlO_2$ counterpart, in agreement with results reported in the literature,[12,26] the Sc- and Y-compounds are advantageous owing to their capacity for acceptor doping. $CuSc_{1-x}Mg_xO_2$ ($x = 0$, 0.01, 0.02, 0.03, and 0.05) samples were synthesized to study the solubility limit of Mg in $CuScO_2$. XRD powder patterns indicate phase-pure samples at all doping levels indicating < ~3% second phase (e.g., MgO); however, further solubility investigations were made with room-temperature electrical conductivity and thermopower measurements. The results are shown in Figure 8, in which the hole concentrations were determined from the thermoelectric coefficients as per eq 5. The errors illustrated for the conductivity and hole concentration values are described by eq 2, whereas error in composition (estimated from inaccuracy in weight measurements) is on the order of symbol size. From Figure 8 the solubility limit is estimated to be ~1%. Furthermore, the hole concentration at saturation is consistent with 1% doping (i.e., $\log(p) = 20.3$), predicted by

$$[Mg_{Sc}^{\bullet}] = p \qquad (9)$$

Since the inclusion of Mg as a neutral defect or ionically compensated defect could not be ruled out, lattice parameter determinations were made through Rietveld refinements of X-ray diffraction patterns using the software package FullProf 2000.[19] Based on Vegard's law analysis of lattice parameters, the Mg solubility limit is confirmed to be approximately 1%, as seen in Figure 9. The electrical properties do not change significantly over 1% Mg-doping (as seen in Figure 8), therefore changes in cation ratios are not expected.

Although Nagarajan et al.[17] report Mg doping of 2.5% in thin films of $CuScO_{2+\delta}$, the above results suggest that the solubility limit is somewhat less in bulk specimens.

(25) Cotton, F. A.; Wilkinson, G. *Advanced Inorganic Chemistry*, 5th ed. Wiley-Interscience: New York, 1988; p 495.
(26) Benko, F. A.; Koffyberg, F. P. *Can. J. Phys.* **1985**, *63*, 1306−1308.

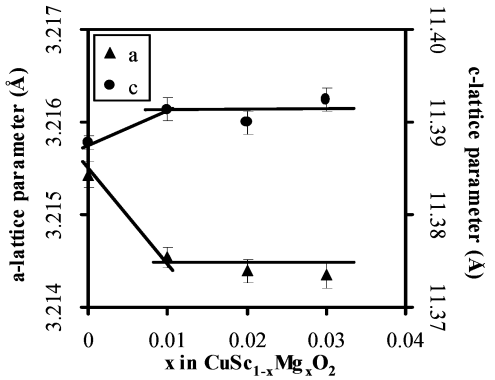

Figure 9. Lattice parameter of $CuSc_{1-x}Mg_xO_2$ as a function of x. Saturation of the electrical properties is attained between $x = 0.1$ and 0.2. The estimated error in x is found to be on the order of symbol size.

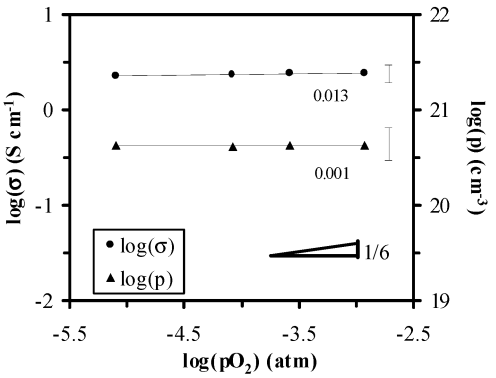

Figure 10. pO_2-Dependence of the electrical properties of 5% Mg-doped $CuScO_2$. The systematic error is represented by the error bar to the right of the data, whereas the random error is on the order of symbol size. The slopes are given by the numerical values and a $^1/_6$ slope is displayed for comparison.

As mentioned above, there is very good agreement between the Mg solubility limits in $CuScO_2$ determined by electrical property and lattice parameter measurements. Both methods suggest a solubility limit of approximately 1%, corresponding to a hole concentration of $\sim 1.96 \times 10^{20}$ cm^{-3} (log(p) = 20.3), in $CuScO_2$ according to eq 9.

The high-temperature pO_2-dependence of the electrical properties of Mg-doped $CuScO_2$ is shown in Figure 10 for $CuSc_{0.95}Mg_{0.05}O_2$, which ensures doping saturation. It should be noted, as seen in Figures 8 and 9, there is little variation in the electrical properties with a small amount of MgO second phase. As seen in Figure 10 the conductivity and hole concentration exhibit nearly oxygen-independent character, indicating that the hole concentration is set by the acceptor doping, as in eq 9. At the same time there is a substantial increase in hole concentration (4.5×10^{20} cm^{-3}) over the undoped material (4.5×10^{19} cm^{-3}), as summarized in Figure 7.

The high-temperature electrical properties of $CuY_{0.95}Ca_{0.05}O_2$ are shown in Figure 11. Second phases (e.g., CaO) were undetectable in XRD analysis, but are assumed to exist in small proportions. As in the Sc-system, there is a significant increase (3.6×10^{18} cm^{-3} to 3.3×10^{19} cm^{-3}) in the hole concentration relative to the undoped compound, however the hole concentration remains low relative to $CuAlO_2$ and doped-$CuScO_2$, as summarized in Figure 7.

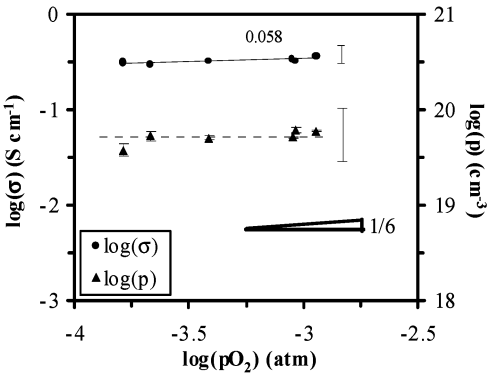

Figure 11. pO_2-Dependence of the electrical properties of 5% Ca-doped $CuYO_2$. The systematic error is represented by the error bar to the right of the data, whereas the random error is on the order of symbol size. The slopes are given by the numerical values and a $^1/_6$ slope is displayed for comparison.

There was significant random error in the thermopower measurements in Figure 11, therefore a horizontal dashed line is used to show the suggested pO_2 dependence. This increase in error relative to similar analyses (e.g., $CuAlO_2$ and $CuScO_2$) was repeatable and is most likely due to the instability of Ca-doped $CuYO_2$ at high-temperatures, as determined through X-ray analysis on specimens removed from measurement conditions.

Figure 7 details the approximate hole concentrations obtained for 1 and 5% doping levels. It is clearly seen that both the 5%-doped $CuScO_2$ and $CuYO_2$ compounds exhibit hole contents less than expected based upon the doping level, most likely due to limited solubility as discussed above.

According to Figure 7, Ca appears to have a lower solubility limit in $CuYO_2$ than Mg in $CuScO_2$, based upon the smaller hole contents registered by Seebeck coefficients measurements. From the hole concentration for Ca-doped $CuYO_2$ (3.3×10^{19} cm^{-3}) and the Y-site density (1.63×10^{22} cm^{-3}), a solubility limit can be estimated to be $\sim$0.2%. It is common for the solubility of dopants in films to be larger than that in bulk specimens. For example, Jayaraj et al. reported optimal Ca doping levels in $CuYO_2$ thin films of 1−2%, leading to a conductivity >0.3 S/cm.[27] The ability to acceptor dope these materials appears to be constrained in bulk specimens, but may be used to advantage in films.

Additional analysis based upon the small polaron model, in which the conductivity is expressed as (from eq 3)

$$\sigma = pe\mu = \frac{gNc(1-c)e^2a^2\nu}{k_BT}\exp\left(\frac{-E_h}{k_BT}\right) \qquad (10)$$

provides an upper bound on the conductivity of these materials. The geometric factor, g, is on order of unity; N is approximately 3×10^{22} cm^{-3}; the product of Na^2 is nearly a constant $\sim 2.03 \times 10^7$ cm^{-1} in the cuprous-delafossites; and ν is on the order of 10^{13} s^{-1}. By assuming a generous doping level of $c = 0.05$ and a negligibly small hopping energy, a value of $\sigma_{max} \approx 75$

(27) Jayaraj, M. K.; Draeseke, A. D.; Tate, J.; Sleight, A. W. *Thin Solid Films* **2001**, *397*, 244−248.

S cm^{-1} is obtained at 300 K. A nonzero value for E_h will further reduce the conductivity.

The defect model changes from primarily cation off-stoichiometry in $CuAlO_2$ ($p = 2[(B_{Cu}^{\bullet\bullet}2O_i'')'']$), as shown in Part 1,[1] to extrinsic acceptor doping (e.g., $CuScO_2$ and $CuYO_2$). At 40 S cm^{-1}, $CuScO_2$ has the highest reported conductivity value for delafossite materials.[17] This can be understood by considering the overall electroneutrality condition:

$$p = [V_{Cu}'] + 2[(B_{Cu}^{\bullet\bullet}2O_i'')''] + [A_B'] + 2[O_i''] \quad (11)$$

The present work showed no evidence for copper vacancies as majority defects in cuprous delafossites. As reported in Part 1,[1] hole generation in $CuAlO_2$ is limited to cation nonstoichiometry (the second term of eq 11); extrinsic acceptor-doping (third term) and oxygen doping (fourth term) appear to be negligible. In contrast, $CuScO_2$ and $CuYO_2$ do not appear to favor cation off-stoichiometry (second term of eq 11), due to cation size and coordination reasons. Extrinsic acceptor doping (third term) is possible, although to a lesser extent in $CuYO_2$ than in $CuScO_2$. Furthermore, both systems are better able to accommodate isolated oxygen interstitials (fourth term), as evidenced by slightly increased pO_2 dependences in Figures 5 and 6. Although not the dominant hole-generation mechanism at high-temperature, oxygen doping is known to play a significant role in the hole-doping of $CuScO_2$ and $CuYO_2$ films at lower temperatures. Because $CuScO_2$ is susceptible to both extrinsic acceptor-doping (third term) and oxygen-doping (fourth term), it boasts the highest reported conductivity (~40 S/cm) at room-temperature.[17]

Conclusions

The defect and transport mechanisms of $CuScO_2$ and $CuYO_2$ were investigated in this study and related to those of $CuAlO_2$ discussed in Part 1.[1] The cuprous-based delafossite class of materials, $CuBO_2$ (B = Al, Sc, and Y) universally adopts a small polaron hopping mechanism for hole conduction; however, the defect model is highly dependent on the size of the B-cation. The electrical properties, including conductivity and thermopower, of the materials tested between 550 and 900 °C agreed with an activated small polaron mobility model as seen by constant (or in some cases decreasing) hole concentrations compared to increasing conductivity with increasing temperature. Furthermore, small polaron conduction was verified in doped $CuScO_2$ and $CuYO_2$ specimens, albeit with increased conductivity due to an increase in hole concentrations relative to undoped samples. Low dopant solubility limits in bulk specimens, especially in $CuYO_2$, constrained the extrinsic contributions to the hole concentrations.

The conductivity in $CuScO_2$ and $CuYO_2$, as in $CuAlO_2$, is limited by a thermally activated mobility. $CuScO_2$ is the best candidate for achieving maximum performance among the investigated materials owing to the defects present in $CuScO_2$ (both intrinsic and extrinsic) relative to $CuAlO_2$ (predominantly intrinsic) and $CuYO_2$ (predominantly extrinsic).

Acknowledgment. This work was supported in part under NSF-MRSEC grant DMR-9632472 and under DOE-NREL subcontract XAT-5-33636-02. B.J.I. was additionally supported through a NDSEG fellowship.

CM048982K